Acta Crystallographica Section D
Biological Crystallography
ISSN 0907-4449

The X-ray structure of *Salmonella typhimurium* uridine nucleoside phosphorylase complexed with 2,2′-anhydrouridine, phosphate and potassium ions at 1.86 Å resolution

Alexander A. Lashkov,[a,b] Nadezhda E. Zhukhlistova,[a] Azat H. Gabdoulkhakov,[a] Alexander A. Shtil,[c] Roman G. Efremov,[b] Christian Betzel[d] and Al'bert M. Mikhailov[a]*

[a]A. V. Shubnikov Institute of Crystallography, Russian Academy of Sciences, 59 Leninsky Prospect, 119333 Moscow, Russia, [b]M. M. Shemyakin and Yu. A. Ovchinnikov Institute of Bioorganic Chemistry, Russian Academy of Sciences, 16/10 Miklukho-Maklay Street, 117997 Moscow, Russia, [c]Blokhin Cancer Center, Russian Academy of Medical Sciences, 24 Kashirskoye Shosse, 115478 Moscow, Russia, and [d]Insitute of Biochemistry and Food Chemistry, University of Hamburg, c/o DESY, Notkestrasse 85, 22603 Hamburg, Germany

Correspondence e-mail: amm@ns.crys.ras.ru

Received 3 August 2009
Accepted 23 October 2009

PDB Reference: uridine nucleoside phosphorylase, 3fwp.

Uridine nucleoside phosphorylase is an important drug target for the development of anti-infective and antitumour agents. The X-ray crystal structure of *Salmonella typhimurium* uridine nucleoside phosphorylase (*St*UPh) complexed with its inhibitor 2,2′-anhydrouridine, phosphate and potassium ions has been solved and refined at 1.86 Å resolution (R_{cryst} = 17.6%, R_{free} = 20.6%). The complex of human uridine phosphorylase I (*H*UPhI) with 2,2′-anhydrouridine was modelled using a computational approach. The model allowed the identification of atomic groups in 2,2′-anhydrouridine that might improve the interaction of future inhibitors with *St*UPh and *H*UPhI.

1. Introduction

Uridine nucleoside phosphorylase (UPh; EC 2.4.2.3) catalyzes the transformation of uridine into uracil in the presence of phosphate ions (Paege & Schlenk, 1952). Owing to its key role in the resynthesis of pyrimidine bases, UPh has been the subject of extensive studies as a drug target. Most importantly, uridine resynthesis involving UPh and uracil phosphoribosyltransferase is critical in bacteria (Niedzwicki *et al.*, 1983). In higher organisms UPh is less important because the predominant portion of pyrimidine bases are synthesized *de novo*, whereas a minor pool is produced *via* resynthesis (Niedzwicki *et al.*, 1983). Many bacteria lack thymidine phosphorylase activity; in these species, UPh catalyzes the phosphorolysis of ribopyrimidine and deoxyribopyrimidine nucleosides (Niedzwicki *et al.*, 1983). Inhibition of Uph is lethal in pathogenic parasites such as *Giardia lamblia* and *Schistosoma mansoni* (Jimenez *et al.*, 1989; Beck & O'Donovan, 2008; Lee *et al.*, 1988; el Kouni, Naguib, Niedzwicki *et al.*, 1988). Therefore, UPh inhibitors have potential as antiparasitic drugs.

In humans, UPh is involved in metabolism of pyrimidine-based anticancer agents. The prototypical drug 5-fluorouracil (5-FU) has been important in cancer treatment for several decades (Chandana & Conley, 2009; Kemeny, 1987; Kohne & Lenz, 2009). Pharmacological antagonists of UPh dramatically potentiate the antitumour efficacy of 5-FU and its prodrug capecitabine (Iigo *et al.*, 1990; Matsusaka *et al.*, 2007; Temmink *et al.*, 2006). In addition to their role in cancer therapy, pyrimidine-based antimetabolites, including 5-FU, also synergize with antibacterial drugs in inhibiting the viability of staphylococci (Gieringer *et al.*, 1986; Yamashiro *et al.*, 1986).

El Kouni and coworkers have shown that derivatives of anhydrouridines down-regulate the majority of UPhs in bacteria and protozoa (el Kouni, Naguib, Chu *et al.*, 1988). In the present study, we focus on the mechanism of UPh inhibition by 2,2′-anhydrouridine (ANU). To obtain insight into

Table 1
Data-collection and refinement statistics.

Values in parentheses are for the last shell.

Data collection	
Space group	$P2_12_12_1$
Unit-cell parameters (Å)	a = 88.790, b = 124.070, c = 134.100, $\alpha = \beta = \gamma$ = 90.00
Molecular weight of the hexamer (kDa)	165
No. of amino-acid residues per monomer	253
Molecules per ASU	1 hexamer
Wavelength (Å)	0.803
Resolution (Å)	88.00–1.86 (1.87–1.86)
No. of measurements with $I > -3\sigma(I)$	303063 (4828)
No. of independent reflections	110180 (1827)
Completeness (%)	88.4 (93.6)
$R_{\rm merge}$ (%)	7.7 (41.0)
$R_{\rm meas}$ (%)	9.4 (50.6)
Average $I/\sigma(I)$	10.00 (2.49)
Refinement	
Resolution (Å)	27.99–1.86 (1.908–1.860)
Data cutoff	$\sigma(\lvert F_{\rm o}\rvert) > 0$
No. of reflections in working set	104669 (7966)
Completeness of working set (%)	88.44 (92.61)
No. of reflections in test set	5509 (419)
$V_{\rm M}$ (Å^3 Da^{-1})	2.19
Solvent content (%)	43
No. of protein atoms	109965
No. of water molecules	1015
No. of ANU molecules	3
No. of phosphate groups	3
No. of potassium ions	3

the enzyme–inhibitor interactions as the structural basis of this mechanism, we investigated the spatial organization of the complex of ANU with UPh from *Salmonella typhimurium* (*St*UPh), a bacterium that is pathogenic to humans, domestic animals and poultry, using atomic resolution X-ray data and computer-assisted modelling. Taking advantage of the high homology between *St*UPh and its human orthologue, uridine nucleoside phosphorylase I (*H*UPhI), we performed molecular docking of ANU into the *H*UPhI model. These data may be regarded as a basis for chemical modifications of ANU aimed at the design of enzyme inhibitors with higher affinity and selectivity for the binding sites in human and bacterial UPhs.

2. Methods

All reagents were purchased from Sigma–Aldrich except where specified otherwise.

2.1. Enzyme isolation and purification

Cloning of the structural gene *udp* of *St*UPh, enzyme isolation and purification were performed as described previously (Molchan *et al.*, 1998; Zolotukhina *et al.*, 2003; Mikhailov *et al.*, 1992). The UPh-producing strain *Escherichia coli* BL21 (DE3) was used. Bacterial cells were solubilized in 10 m*M* KH_2PO_4 pH 7.0 containing 1% polyethyleneimine and 0.5 m*M* β-mercaptoethanol and then centrifuged at 15 000*g* for 15 min. The supernatant was incubated at 277 K for 3 h; proteins were then precipitated with polyethylene glycol (PEG) and resuspended in buffer containing 10 m*M* KH_2PO_4 pH 7.2 and 0.5 m*M* β-mercaptoethanol. Further purification of *St*UPh was performed using butyl-Sepharose chromatography and Q-Sepharose chromatography (Dontsova *et al.*, 2004). The homogeneity of the native *St*UPh was determined by electrophoresis in a 7.5% polyacrylamide gel under nondenaturing conditions.

2.2. Crystallization

Crystals were grown by the hanging-drop vapour-diffusion method (Timofeev *et al.*, 2007). The complex of *St*UPh with ANU, phosphate and potassium ions was obtained by co-crystallization. The reservoir solution (1 ml) consisted of 18%(*w*/*v*) PEG 4000 and 0.1 *M* Tris–HCl buffer pH 5.2. The crystallization solution contained 3 µl protein solution (13 mg ml^{-1} in 0.05 *M* Tris–HCl buffer pH 5.2), 3 µl 18%(*w*/*v*) PEG 4000 in 0.05 *M* Tris–HCl buffer pH 5.2, 0.5 µl 10 m*M* ANU and 0.1 µl 1 m*M* KH_2PO_4. Crystals grew at 298 K in one week.

2.3. Data collection and processing

Diffraction data were collected under cryogenic conditions (using glycerol as a cryoprotectant) to 1.86 Å resolution on the Consortium Beamline X13 at DESY, Hamburg, Germany at a wavelength of 0.803 Å. Data were processed and merged using the *XDS* package (Kabsch, 2001). The crystal parameters and data-collection statistics are summarized in Table 1.

2.4. Structure determination and refinement

The crystal structure was solved by the molecular-replacement technique using the *Phaser* program with rigid-body refinement option (McCoy, 2007). The X-ray structure of *St*UPh at 1.64 Å resolution (PDB code 2i8a; V. I. Timofeev, M. V. Dontsova, A. G. Gabdoulkhakov, A. A. Lashkov, V. Voelter, G. S. Kachalova, B. P. Pavlyuk & A. M. Mikhailov, unpublished work) was used as the search model. The atoms of the ligand and water molecules were removed from the model. Only one solution was evident, with an R factor of 26.5% and a correlation coefficient $R_{\rm corr}$ of 84.9%. The structure was subjected to several cycles of simulated-annealing refinement with the *PHENIX* program suite (Adams *et al.*, 2002). A free R factor ($R_{\rm free}$) calculated from 5% of reflections set aside at the outset was used to monitor the progress of refinement. The model bias present in the initial molecular-replacement solution was tackled using cross-validated and $\sigma_{\rm A}$-weighted maps as implemented in *PHENIX*. The *PHENIX* refinement stages were alternated with manual correction of the model. Stereochemical parameters were improved using the *Coot* program (Emsley & Cowtan, 2004) based on weighted electron-density maps with ($\lvert F_{\rm o}\rvert - \lvert F_{\rm c}\rvert$) and ($2\lvert F_{\rm o}\rvert - \lvert F_{\rm c}\rvert$) coefficients. In the final stages of model building, the ANU molecules and the phosphate and potassium ions were localized. When the R factor value reached 20% water molecules were placed into peaks greater than 3σ from $F_{\rm o} - F_{\rm c}$ maps, but only when they were within suitable hydrogen-bonding distance of amino-acid atoms.

Table 2
Statistics of model quality.

Values in parentheses are for the last shell.

R_{factor} (%)	17.6 (24.8)
R_{free} (%)	20.6 (28.7)
$R_{factor+free}$ (%)	17.8
Average *B* values (Å^2)	
Overall	19.5
Main chain	18.9
Side chains	20.2
Water molecules	29.6
ANU molecules	23.2
Phosphate groups	25.2
Potassium ions	18.5
Observed r.m.s.d. from ideal geometry	
Bond lengths (Å)	0.007
Bond angles (°)	1.066
Chirality (Å^3)	0.069
Planarity (Å)	0.003
Error in coordinates from Luzzati plot (Å)	0.188
DPI (Å)	0.132
Ramachandran plot, residues in	
Most favoured regions (%)	89.7
Additionally allowed regions (%)	9.8
Generally allowed regions (%)	0.5
PDB code	3fwp

In the last step of structure refinement, the *REFMAC* program was used with the Restrain and TLS Refinement options (Murshudov *et al.*, 1997). The model, which was ultimately refined to an *R* factor of 17.6% (R_{free} = 20.6%) at 1.86 Å resolution, showed good quality (Tables 1 and 2) as judged by the program *PROCHECK* (Laskowski *et al.*, 1993). The model had no residues in the disallowed regions of the Ramachandran plot (Ramachandran *et al.*, 1963). The structure of *St*UPh has been deposited in the Protein Data Bank (Berman *et al.*, 2003; Bernstein *et al.*, 1977) with PDB code 3fwp.

2.5. Molecular docking and design

The resulting X-ray model of *St*UPh was prepared for further molecular design. H atoms were added automatically and partial atomic charges were assigned. This was performed using the *MAESTRO* program (v.8.0; Schrödinger LLC, New York, USA). The structure of *H*UPhI was obtained from the Protein Data Bank (PDB code 3euf; Roosild *et al.*, 2009). Stereochemical data on the structures of ANU and 5-benzylacyclouridine (BAU) were obtained from the PubChem database (Xie & Chen, 2008). Optimization of ligand binding in the enzyme active site was performed *via* sampling of torsion angles, the addition of H atoms and attributing partial atomic charges using the *PRODRG* web server (Schüttelkopf & van Aalten, 2004).

Molecular docking was performed with the *Glide* program using the Extra Prescription (XP) option with flexible ligand and immobile target (Friesner *et al.*, 2006). The docking sphere (radius 15 Å) was centred at the mass centre of the ANU molecule in the crystal structure of the complex of *St*UPh with ANU and PO_4^{3-}. Default values were used for the other parameters of the docking protocol. The scoring function Glide Score (G-score) was implemented to rank the results of docking. The *in silico* design of new inhibitors was performed using the Combinatorial Screening operation of the program module *CombiGlide* (v.1.5; Schrödinger LLC, New York, USA). The structure of ANU was used as a starting model for *in silico* inhibitor design.

3. Results and discussion

3.1. Overall structure

We recently analyzed the quaternary structure of *St*UPh (Lashkov *et al.*, 2009). The molecule can be represented as a toroid-shaped hexamer formed by six homologous subunits, each with a molecular mass of 27 kDa. These subunits are arranged in the enzyme molecule according to point group 32. The molecule is approximately 51 Å in height and its external diameter is about 108 Å. The channel in the centre of the molecule is 10 Å in diameter and expands to 19 Å at the periphery.

X-ray analysis at 1.5 Å resolution revealed that a single homodimer is the minimal essential constituent of hexameric *St*UPh (Fig. 1). The enzyme forms hexamers in solution and in the crystal (Molchan *et al.*, 1998). Unlike *St*UPh and the *E. coli* orthologue *Ec*UPh, the quaternary structure of *H*UPhI is represented by a homodimer (Roosild *et al.*, 2009). However, in all eukaryotic and prokaryotic UPhs studied to date the homodimer is the major structural and functional unit (Burling *et al.*, 2003; Caradoc-Davies *et al.*, 2004; Dontsova *et al.*, 2004; Roosild *et al.*, 2009).

We have demonstrated that the formation of hexameric *St*UPh from homodimers involves hydrophobic interactions

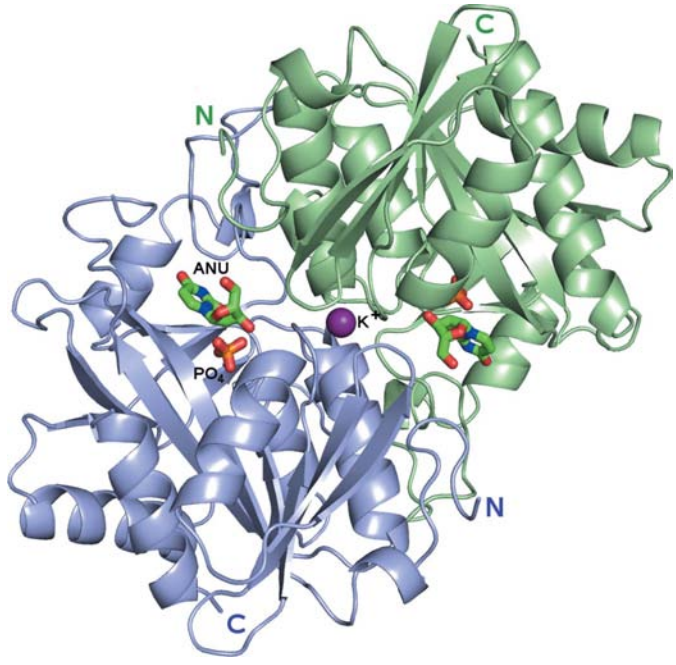

Figure 1
General organization of the *BD* dimer of the complex of *St*UPh with phosphate ion and ANU. The *B* and *D* monomers are shown in green and blue, respectively. The potassium ion in the interdimeric space is rendered as a sphere. The positions of PO_4^{3-} and ANU in the active sites are represented as sticks.

and the creation of a network of hydrogen bonds (Lashkov *et al.*, 2009). The hydrogen bonds between the amino-acid residues of the subunits are linked together by a noncrystallographic axis of third-order symmetry. These bonds, which are located in the central channel of *St*UPh and *Ec*UPh, are 2.7–3.4 Å in length (Lashkov *et al.*, 2009). The intermonomeric interactions within the homodimer include hydrophobic contacts, hydrogen bonds and ion bridges. 20–25 hydrogen bonds are found between the subunits in the homodimer. This varying number of hydrogen bonds can be explained by the fact that the pairs of bond-forming atoms sometimes involve the amino-acid residues of highly flexible loops. The intermonomeric contacts between potential donors and acceptors of hydrogen bonds in the *St*UPh *BD* homodimer are presented in Table 3.

The *St*UPh monomer (253 amino-acid residues; Fig. 2) is an α/β-class polypeptide with a trilayer $\alpha/\beta/\alpha$ sandwich architecture (Fig. 1). Approximately 33% of the tertiary structure of the subunit is represented by helical structures, whereas 20% consists of β-strands (*PROCHECK*; Laskowski *et al.*, 1993).

3.2. The potassium ion

This ion is located in the intermonomeric region of each homodimer on the local axis of second order of point group 32 of *St*UPh (Fig. 1). The side chains of Glu49*B* and Ser73*B* and the carbonyl O atom of Ile69*B* in the *B* subunit, as well as symmetrical residues from the *D* subunit of the *BD* homodimer, coordinate K^+. The atoms that interact with K^+, namely Glu49*B* OE2, Ile69*B* O, Ser73*B* OG, Glu49*D* OE1, Ile69*D* O and Ser73*D* OG (Fig. 3), form a distorted octahedron or a triangular prism. The distances between K^+ and the surrounding O atoms are Glu49*B* OE2–K^+, 2.66 Å; Ile69*B* O–K^+, 2.82 Å; Ser73*B* OG–K^+, 2.86 Å; Glu49*D* OE1–K^+, 2.75 Å; Ile69*D* O–K^+, 2.78 Å; Ser73*D* OG–K^+, 2.86 Å. Similar bonds between K^+ and adjacent atoms (in terms of configuration and length) are found in the *AF* and *CE* homodimers. Matching the *BD* and *AF* homodimers and the *BD* and *CE* homodimers revealed root-mean-square deviations (r.m.s.d.s) in bond distances between K^+ and the atoms of the coordination sphere of 0.11 and 0.17 Å, respectively. In all homodimers one water molecule is bound to Ile69 O of the neighbouring subunits in the vicinity of each K^+. In the *BD* homodimer the lengths of the hydrogen bonds are 2.75 Å for Ile69*B* O–H_2O and 2.57 Å for Ile69*D* O–H_2O.

Studies of *Ec*UPh have demonstrated that K^+ increases the enzymatic activity (Caradoc-Davies *et al.*, 2004). Our comparison of the spatial structure of unliganded *St*UPh with and without K^+ led us to conclude that K^+ stabilizes the spatial structure of unliganded substrate binding sites in an open or an intermediate conformation of the active site (Lashkov *et al.*, 2009). Because of the high homology between *St*UPh and *Ec*UPh, it is probable that K^+ indirectly influences the enzymatic activity by stabilizing the L2 loop in the open conformation (Lashkov *et al.*, 2009; Figs. 1 and 2). In this case, the binding sites in the active centre of the *St*UPh homodimer would be better accessible to the substrate than if the enzyme contained no K^+. In the structures of *H*UPhI complexed with BAU no K^+ ion was detectable in the intermonomeric region of the homodimer (Roosild *et al.*, 2009).

3.3. The active site

Each homodimer of the hexameric *St*UPh molecule possesses two active sites (Fig. 1; Lashkov *et al.*, 2009). The phosphate and nucleoside binding centres in the active site are formed by amino-acid residues from both subunits of the homodimer (Fig. 4). However, the number of active-site-forming amino-acid residues from one subunit is larger than that from the other subunit. We designated the binding sites by the name of the subunit with the maximal number of amino-acid residues. The $F_o - F_c$ electron-density map shows

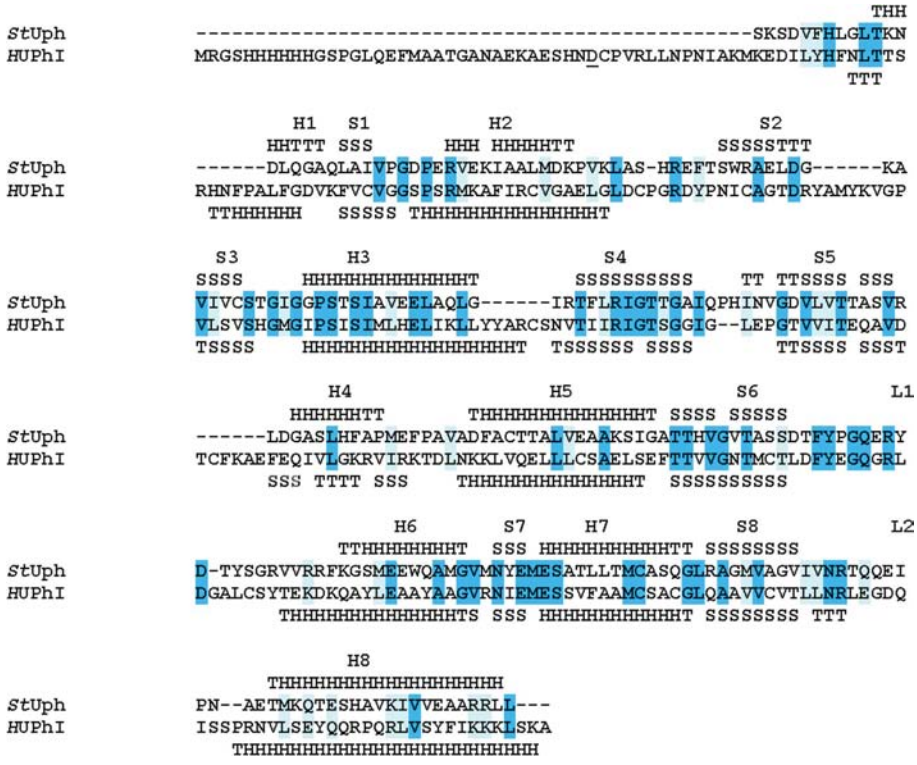

Figure 2
Alignment of the amino-acid sequences of *St*UPh and *H*UPhI together with secondary-structure information from X-ray three-dimensional structures. S, strand; H, helix; T, turn. The alignment was produced using *ClustalW*2 (Larkin *et al.*, 2007). The secondary-structure information was obtained using *PROCHECK* (Laskowski *et al.*, 1993). Fully conserved residues are shaded dark blue and nonconserved residues are unshaded.

an absence of PO_4^{3-} and ANU in the substrate binding sites of the *CE* homodimer. In the *BD* homodimer both sites are occupied by PO_4^{3-} and ANU. In the *AF* homodimer the binding sites in the *A* subunit are unliganded, whereas a phosphate ion and ANU are present in the binding sites of the *F* subunit of the same homodimer.

3.3.1. The phosphate binding site. Fig. 1 shows the active site of the *B* subunit of the *BD* homodimer with PO_4^{3-} (in the phosphate binding site) and ANU (in the nucleoside binding site). The residues in the phosphate binding site are Arg30*B*, Arg91*B*, Thr94*B* and Gly26*B* from the *B* subunit, and Arg48*D* from the *D* subunit. The O atoms of PO_4^{3-} form one or two hydrogen bonds to each of these residues (Fig. 4), namely Arg48*D* NH2$\cdots$$PO_4$ O2, 2.91 Å; Arg48*D* NH1$\cdots$$PO_4$ O3, 2.96 Å; Arg30*B* NH2$\cdots$$PO_4$ O2, 2.68 Å; Arg30*B* NH1$\cdots$$PO_4$ O1, 2.67 Å; Arg91*B* NH1$\cdots$$PO_4$ O1, 3.2 Å; Arg91*B* NH1$\cdots$$PO_4$ O4, 2.82 Å. The OH-group O atom of the side chain of Thr94 (Thr94*B* OG1–PO_4 O2, 2.62 Å) and the N atom of the main chain of Gly26 (Gly26*B* NH–PO_4 O1, 2.81 Å) interact with the phosphate ion. The latter forms a hydrogen bond to ANU (ANU O3′$\cdots$$PO_4$ O3, 2.68 Å) (Fig. 4).

The Arg residues are linked to PO_4^{3-} owing to strong electrostatic interactions between the positively charged amino groups of the side chains (Arg48*D* NH2, Arg48*D* NH1, Arg30*B* NH2, Arg30*B* NH1, Arg91*B* NH1, Arg91*B* NH2) and the negatively charged O atoms of the phosphate ion. Considering the active site of the *C* subunit, which is not bound to PO_4^{3-}, the position of the side chain of Arg30*B* (r.m.s.d. = 4.05 Å) has changed drastically compared with the position of Arg30*C*. The atomic positions of the side chains of other residues changed to a lesser extent: the r.m.s.d. of Arg91*B* compared with Arg91*C* is 1.60 Å and that of Arg48*D* compared with Arg48*E* is 1.95 Å. The main-chain atoms of Arg30*B* (r.m.s.d. 0.31 Å), Arg91*B* (r.m.s.d. 0.24 Å) and Arg48*D* (r.m.s.d. 0.11 Å) remain at the same positions as the corresponding atoms of the residues in the unliganded active site of the *C* subunit.

Table 3
Intermonomeric contacts in the *BD* homodimer of *St*UPh.

B subunit atom	*D* subunit atom	Distance (Å)
Glu49 OE2	Ile69 N	2.77
Ile69 N	Glu49 OE1	2.81
Glu79 OE1	Tyr172 N	2.81
Glu80 OE2	Tyr163 OH	2.69
Arg87 NE	Tyr172 OH	3.28
Leu116 O	His122 NE2	2.97
Ala119 N	Asp160 OD1	3.22
His122 ND1	Thr161 OG1	2.73
His122 NE2	Leu116 O	3.03
Phe123 O	Arg175 NH1	2.78
Phe123 O	Arg175 NH2	2.91
Phe123 O	Ala119 N	3.21
Phe123 O	Asp160 OD1	3.13
Thr161 OG1	His122 ND1	2.72
Tyr163 OH	Glu80 OE2	2.62
Tyr172 N	Glu79 OE1	2.75
Tyr172 OH	Arg87 NE	3.36
Ser173 OG	Gln209 OE1	3.14
Ser208 OG	Arg175 NH2	3.21
Ser208 O	Arg175 NH2	3.12
Gln209 NE	Ser173 OG	2.88

Superposition of the three-dimensional structures of the phosphate binding sites in *St*UPh and *H*UPhI (Roosild *et al.*, 2009) liganded with PO_4^{3-} reveals similarities in their spatial architecture. In *H*UPhI the phosphate binding site is represented by Arg138, Arg64, Thr141 and Arg194 from an adjacent subunit of the same homodimer. For these residues the position of the main chain coincides with the direction of the main chain of the residues in the phosphate binding site of *St*UPh. Pairwise comparison of the main-chain atoms gives r.m.s.d.s of 0.65 Å for Arg138*A* in *H*UPhI *versus* Arg91*B* in *St*UPh, 0.66 Å for Arg64*A* in *H*UPhI *versus* Arg30*B* in *St*UPh, 0.79 Å for Thr141*A* in *H*UPhI *versus* Thr94*B* in *St*UPh and

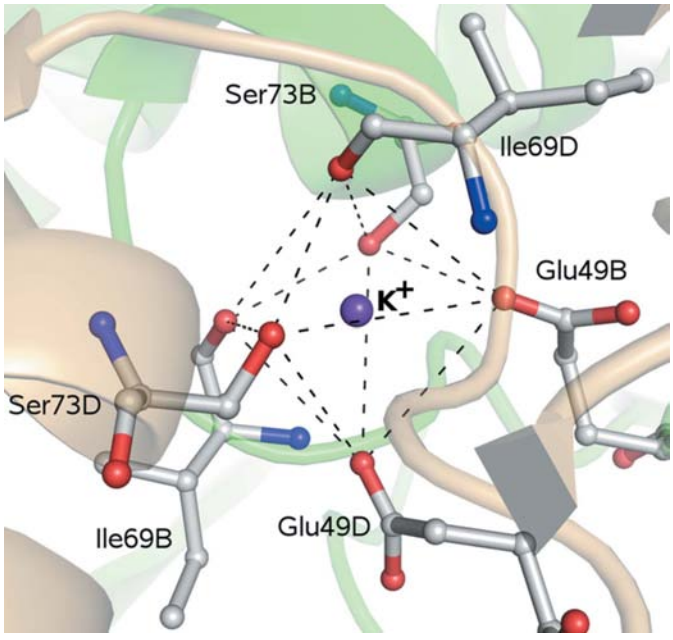

Figure 3
The potassium ion surrounded by amino-acid residue atoms. The K^+ ion is shown as a ball. The residues of the neighbouring atoms are shown in ball-and-stick representation. The dotted lines show the irregular prism formed by the adjacent atoms.

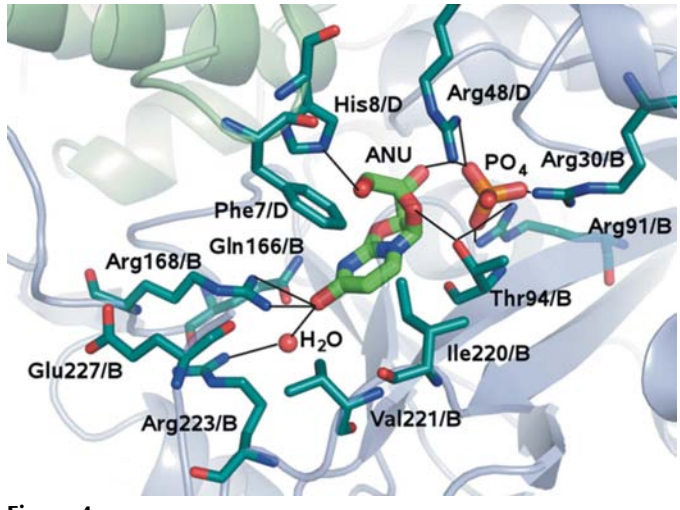

Figure 4
ANU and PO_4^{3-} in the active site of *St*UPh. The major amino-acid residues in the active site and the ligands are shown as sticks. Solid black lines show hydrogen bonds.

1.01 Å for Arg94*B* in *H*UPhI *versus* Arg48*D* in *St*UPh. Larger deviations of the atomic positions in the main chain might arise from a higher mobility of the monomers in *H*UPhI than in *St*UPh. Comparison of the *H*UPhI *A* subunit and the *St*UPh *B* subunit in the complexes with PO_4^{3-} and ANU shows a coincidence of the side chains of Arg138*A* in *H*UPhI with Arg91*B* in *St*UPh (r.m.s.d. = 0.56 Å), Thr141*A* in *H*UPhI with Thr94*B* in *St*UPh (r.m.s.d. = 0.86 Å) and Arg94*B* in *H*UPhI with Arg48*D* in *St*UPh (r.m.s.d. = 1.43 Å). A significant difference is detected for the side-chain atoms of Arg64*A* in *H*UPhI compared with Arg30*B* in *St*UPh (r.m.s.d. = 3.63 Å). Thus, the side chain of Arg64*A* in *H*UPhI is not bound to PO_4^{3-}. Supposedly, this difference is a consequence of the influence of Gln296 in *H*UPhI, with which Arg64 forms a hydrogen bond (Arg64*A* NH1···Gln296*A* OE1 = 2.96 Å in *H*UPhI). However, Arg64 in *H*UPhI could bind PO_4^{3-} if this residue formed a rotamer similar to that of Arg30 in *St*UPh.

3.3.2. The uracil binding site. The key residues that interact with uracil in *St*UPh are Gln166*B*, Arg168*B* and Arg223*B*. These residues are conserved in bacterial phosphorylases and are important for recognition of the pyrimidine ring in substrates (Burling *et al.*, 2003; Dontsova *et al.*, 2004; Morgunova *et al.*, 1995). In the uracil binding site, O4 of the uracil moiety of ANU and the respective atom in BAU form hydrogen bonds to the same atoms (Bu *et al.*, 2005). In *Ec*UPh the O4 atom of the inhibitor forms hydrogen bonds to Arg168*B* (Arg168*B* NH1···ANU O4, 3.24 Å; Arg168*B* NH2···ANU O4, 2.82 Å; Caradoc-Davies *et al.*, 2004) and with the side chain of Arg223*B* through water molecules (ANU O4···HOH, 2.60 Å; Arg223*B* NH1···HOH, 3.11 Å). The N3 atom of ANU is not bound to the OE1 atom of the side chain of Gln166. This differs from the binding of BAU and related inhibitors because the pyrimidine ring is fixed in the *syn* conformation in ANU (Bu *et al.*, 2005). Furthermore, no hydrogen bond is detectable between ANU O2 and NE2 of the side chain of Gln166, whereas Gln166*B* OE1 is bound to the O4 atom of ANU (Gln166*B* OE1–ANU O4, 3.05 Å). A hydrogen bond is formed between Gln166*B* NE2 and the N3 atom of ANU (Gln166*B* NE2···ANU N3, 3.39 Å).

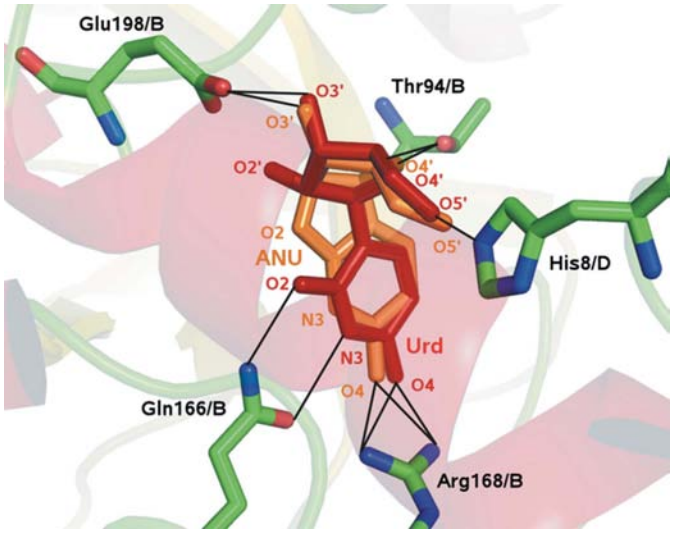

Figure 5
Positions of ANU and uridine in the nucleoside binding site of *St*UPh. The major amino-acid residues in the active site and the ligands are shown as sticks. ANU is coloured orange and uridine is coloured red. Solid lines show hydrogen bonds.

A comparison of the residues of unliganded uracil binding sites demonstrates high homology between *H*UPhI and *St*UPh. The r.m.s.d. values between the coordinates of the main-chain atoms are 0.18 Å for Gln217*A* in *H*UPhI *versus* Gln166*B* in *St*UPh, 0.56 Å for Arg219*A* in *H*UPhI *versus* Arg168*B* in *St*UPh and 0.43 Å for Arg275*A* in *H*UPhI *versus* Arg223*B* in *St*UPh. The respective values for the side-chain atoms are 0.47 Å for Gln217*A* in *H*UPhI *versus* Gln166*B* in *St*UPh, 0.75 Å for Arg219*A* in *H*UPhI *versus* Arg168*B* in *St*UPh and 0.40 Å for Arg275*A* in *H*UPhI *versus* Arg223*B* in *St*UPh.

The hydrophobic area surrounding the ANU pyrimidine ring in *St*UPh includes Gly96*B*, Phe162*B*, Ile220*B* and Val221*B* (Fig. 4). The most hydrophobic residues Ile220*B* and Val221*B* are close to position 5 of the ANU pyrimidine ring. In *H*UPhI the hydrophobic region around the inhibitor is formed by Gly143*A*, Phe213*A*, Leu272*A* and Leu273*A*. The hydrophobicity of these residues is similar in the bacterial and human enzymes and the r.m.s.d. value between the coordinates of the main-chain atoms (calculated for the respective atoms matched pairwise) is <0.95 Å.

In the closed active centre the side chain of Phe7*D* of the neighbouring monomer prevents access of the solvent to the uracil binding site. This residue is also close to position 5 of the uracil ring of the inhibitor (Fig. 4). The angle between the phenyl ring of Phe7 and ANU in the *St*UPh–ANU complex is ∼30°, unlike the respective angle in the *Ec*UPh–BAU complex and the position of the side group of the analogous residue Tyr35*D* in the *H*UPhI–BAU complex (Roosild *et al.*, 2009). We attribute this to van der Waals interactions between the side chains of Phe7 (*Ec*UPh) and Tyr35 (*H*UPhI) and the atoms of the phenyl ring of BAU.

3.3.3. The ribose binding site. In *St*UPh the binding site for the ANU ribose group is located between the uracil and phosphate binding centres (Fig. 4). The hydroxyl group at position 3 of the ribose moiety forms hydrogen bonds to the side chain of Glu198*B* (Glu198*B* OE2···ANU O3′, 2.42 Å; Glu198*B* OE1···ANU O3′, 3.03 Å). In the complexes of *Ec*UPh or *H*UPhI with acyclouridines this residue is bound to water. In *St*UPh, His8*D* from the neighbouring monomer forms a hydrogen bond to the 5′-hydroxyl of the ANU ribose moiety (His8*D* NE2···ANU O5′, 2.68 Å) similar to that in the *Ec*UPh–BAU complexes (Bu *et al.*, 2005). The hydroxyl group of the Thr94*B* side chain of *St*UPh forms hydrogen bonds to PO_4^{3-} and the O4′ atom of the ANU carbohydrate moiety (Thr94*B* OG1···ANU O4′, 3.03 Å). The S atom in Met197*B* of *St*UPh stabilizes the positions of ribose, uridine and ANU *via* van der Waals interactions with the atoms of the furanose ring (C1′-C2′-C3′-C4′-O4′; Fig. 5). These data indicate that the ribose moiety of ANU binds to *St*UPh in a similar manner to the binding of physiological substrates, unlike the binding of acyclouridines, which contain C1′-O2′-C3′-C4′-O5′ instead of ribose.

The primary and tertiary protein structures of the ribose binding sites of *H*UPhI (Roosild *et al.*, 2009) and *St*UPh are homologous. Pairwise comparison of the coordinates of the backbone atoms reveals the following r.m.s.d. values: 0.33 Å for Glu250*A* in *H*UPhI *versus* Glu198*B* in *St*UPh, 0.36 Å for His36*B* in *H*UPhI *versus* His8*D* in *St*UPh and 0.16 Å for Met249*A* in *H*UPhI *versus* Met197*B* in *St*UPh. The respective r.m.s.d. values for side-chain atoms are 0.52 Å for Glu250*A* in *H*UPhI *versus* Glu198*B* in *St*UPh, 0.50 Å for His36*B* in *H*UPhI *versus* His8*D* in *St*UPh and 0.40 Å for Met249*A* in *H*UPhI *versus* Met197*B* in *St*UPh.

3.3.4. Role of the L2 loop. The active centre can adopt an open, an intermediate or a closed conformation depending on the presence of substrates (Caradoc-Davies *et al.*, 2004). The L2 loop in *St*UPh formed by residues 223–233 (Fig. 2) can open or close access of the solvent and ligands to the active site. The loop conformation in the *St*UPh *B* subunit (closed active site) is fixed by hydrogen bonds and salt bridges between Glu227*B* and Arg168*B* (Arg168*B* NE–Glu227*B* O, 2.80 Å; Arg168*B* NH2–Glu227*B* O, 2.73 Å), Tyr169*B* (Tyr169*B* N–Glu227*B* OE2, 2.71 Å) and Asp170*B* (Asp170*B* N–Glu227*B* OE1, 2.93 Å). A similar position of Glu227 has been reported for the closed active site in *Ec*UPh (Caradoc-Davies *et al.*, 2004). In the closed active centres of *Ec*UPh and *St*UPh residues 230–238 are disordered. In the open active site, *e.g.* in the *A* subunit of *St*UPh, Glu227*A* is exposed to the solvent and interacts with water molecules. Because the active site in the *A* subunit is free from substrate, one can suppose that the loop acts as a gatekeeper for the substrates and products of enzymatic catalysis. The positioning of the loop in the complex of the enzyme with PO_4^{3-} and ANU is probably regulated by interaction of the inhibitor with amino-acid residues of all three binding sites simultaneously. Such a mode of interaction resembles the binding of *Ec*UPh to acyclo-ribonucleoside inhibitors and PO_4^{3-}, as well as to some substrates and pseudo-substrates (Bu *et al.*, 2005; Caradoc-Davies *et al.*, 2004).

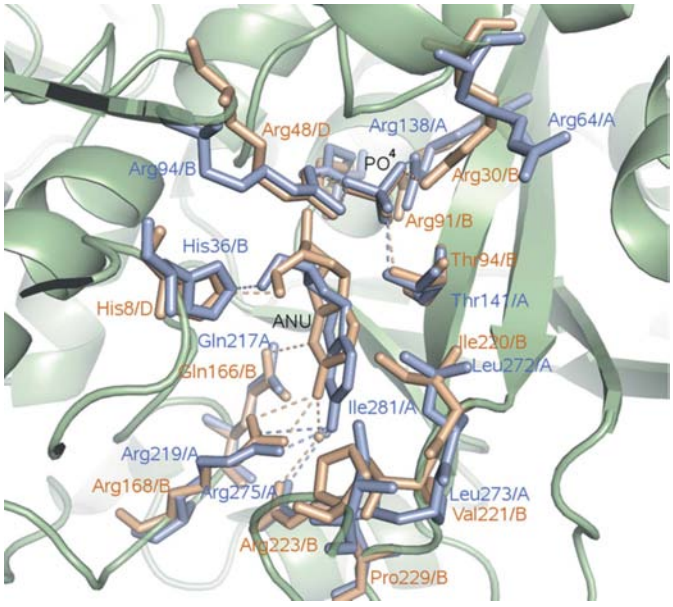

Figure 6
Positions and conformations of ANU and PO_4^{3-} in the active centres of *St*UPh and *H*UPhI. The major residues in the active site of *St*UPh are shown as yellow sticks. The major residues in the active site of *H*UPhI are shown as blue sticks.

In *H*UPhI the L2 loop (Fig. 2) is formed by residues 275–284 (Roosild *et al.*, 2009). Taking into consideration all the structures of *H*UPhI analyzed by Roosild and coworkers, as well as the structures of bacterial phosphorylases (Caradoc-Davies *et al.*, 2004), one may argue that the position of the loop remains closed regardless of the ligands in the active centre. Asp279, which corresponds to Glu227 in *St*UPh, forms hydrogen bonds to amino-acid residues in all *H*UPh structures. In the structure of the *H*UPhI *C* subunit complexed with BAU, Asp279 forms the following hydrogen bonds: Asp279*A* OD1···Arg275*A* NE, 3.12 Å; Asp279*A* OD1···Arg275*A* NH2, 3.09 Å; Asp279*A* OD2···Leu220*A* N, 2.75 Å. Unlike in *St*UPh, in *H*UPhI the similarity of the spatial positioning of the loop residues in different subunits is high. The r.m.s.d. values for the coordinates of the C^{α} atoms in the L2 loops of *H*UPhI monomers are 0.15–0.25 Å, whereas in *St*UPh this parameter exceeds 1.8 Å. In the unliganded *H*UPhI the L2 loop is also in a position similar to its position in the closed active centre. We explain this fact as arising from the influence of the sulfate ion that is nonspecifically bound to the active site in *H*UPhI (PDB code 3eue; Roosild *et al.*, 2009).

3.4. Mechanism of enzyme inhibition

The inhibitory effect of ANU on UPh requires interaction of the drug with the residues in the nucleoside binding site. As shown above, the bonds formed by the ribose moiety of the inhibitor in the active site are critical for drug–enzyme binding. Residues Thr94*B*, His8*D* and Glu198*B* (Figs. 4 and 5) form hydrogen bonds to the inhibitor that resemble the bonds to the ribose of uridine. Arg166*B* also participates in the binding by establishing a contact with O4 of ANU.

During the enzymatic reaction, Gln166 and Arg168 of *St*UPh are involved in a redistribution of electron density from O4′ of the ribose in uridine to the pyrimidine ring. As a result, the oxocarbenium ion is stabilized by a negatively charged phosphate ion. The latter is bound on the α side of the ribose ring where the ion can participate in S_N1 nucleophilic attack at the C1′ position (Caradoc-Davies *et al.*, 2004). In contrast to the mode of binding of the physiological substrate, in the case of ANU binding the N-glycoside bond remains stable owing to fixation of the ANU pyrimidine ring in the *syn* position by O2 and different positioning of the uracil ring relative to Glu168 and Arg166 (Fig. 5). Since the structures of the active sites of *H*UPhI and *St*UPh are highly homologous, it is plausible to suggest that the mechanisms of ANU binding and inhibition of the human enzyme resemble those described for the bacterial counterpart (Caradoc-Davies *et al.*, 2004).

3.5. *In silico* design of new inhibitors

3.5.1. Docking of ANU into *H*UPhI. We designed tentative inhibitors of *St*UPh and *H*UPhI using a multi-step molecular-modelling approach. The computational protocol was vali-

dated by docking ANU into the active site of the *B* subunit (Fig. 1) on the basis of the X-ray structure of *St*UPh. The resulting conformations of the complex are compared with the experimental data obtained in this study. ANU was omitted from the crystal structure before docking. The top-ranked docking solution with minimal G-score (−5.53) is close to the position of the ligand in the crystal structure (r.m.s.d. < 0.5 Å). To test the computational approach on the apoenzyme (crystallized without a ligand), ANU was docked into the active site of an unliganded *A* subunit in which the position of the L2 loop corresponded to the open conformation of the active site. Two very similar solutions were obtained that differed only in the positions of the hydroxyl group at the C5′ atom of the ribose moiety.

Superposition of the active sites on C^{α} atoms (obtained by docking ANU into the binding sites of the *A* and *B* subunits of the *St*UPh crystal structure) shows that the positions of ANU are almost identical (r.m.s.d. <0.6 Å). ANU forms hydrogen bonds to residues in the binding sites that are analogous to those found in the crystal structure (ANU_{dock} O4···Arg168*A* NH2, 2.97 Å; ANU_{dock} O5′···His8*F* NE2, 3.04 Å; ANU_{dock} O3′···Glu198*A*, 3.40 Å). These data can be explained by minor conformational changes in the binding sites upon enzyme–ligand interaction (see above). Thus, the docking of ANU into *St*UPh based on the X-ray structure of the complex with ANU and PO_4^{3-} validates our modelling procedures.

Finally, we docked ANU into the active site of the *A* subunit of the *H*UPhI *AB* dimer. Two similar solutions were generated by the docking procedure. Comparison with the crystal structure of the *St*UPh–ANU complex revealed that the conformations of the inhibitor were similar (Fig. 6). The hydrogen bonds between ANU and the binding sites of the *H*UPhI model are formed by the same residues as in the *St*UPh structure: ANU_{dock} O4···Arg219*A* NH2 of *H*UPhI, 2.63 Å; ANU O4···Arg168*B* NH2 of *St*UPh, 2.82 Å; ANU_{dock} O5′···His36*B* NE2 of *H*UPhI, 2.91 Å; ANU O5′···His8*D* NE2 of *St*UPh, 2.68 Å). These calculations further substantiate the high structural homology between the binding sites in *H*UPhI and *St*UPh. A small difference in the positioning of ANU might be explained by the substitutions of Pro229 in *St*UPh by Ile226 in *H*UPhI, of Ile220 in *St*UPh by Leu257 in *H*UPhI and of Val221 in *St*UPh by Leu258 in *H*UPhI in the *St*UPh *B* subunit and the *H*UPhI *A* subunit loops in positions that correspond to the closed active site. These residues are in close proximity to the C5 atom of the ANU uracil ring and the aforementioned substitutions change the configuration of the hydrophobic pocket in the active site. This in turn shifts ANU in the modelled *H*UPhI complex compared with the X-ray structure of the *St*UPh–ANU complex.

3.5.2. Design of new ANU-based UPh inhibitors. Based on X-ray analysis of the complexes of *St*UPh with ANU and PO_4^{3-}, it may be tentatively suggested that the substituents at position 5 of the ANU pyrimidine ring should be short hydrophobic chains. These moieties are capable of interacting with the hydrophobic pocket near C5 of the pyrimidine ring and the aromatic group that would form stacking interactions with Phe162 and Phe7 of the neighbouring monomer. However, the conformation of the loop and the terminal α-helix adopted when the active site is closed could hamper the binding of an inhibitor with a bulky substituent at position 5 of the uracil ring. We picked optimal substituents from a library of 146 functional groups using *CombiGlide*. Docking grids were obtained for *H*UPhI and *St*UPh, with the latter having two possible states of the active centre and two respective positions of the functional loop. For *H*UPhI only one state of the active centre and the loop was detectable in the crystal structures of the complexes with sulfate ion and BAU (Roosild

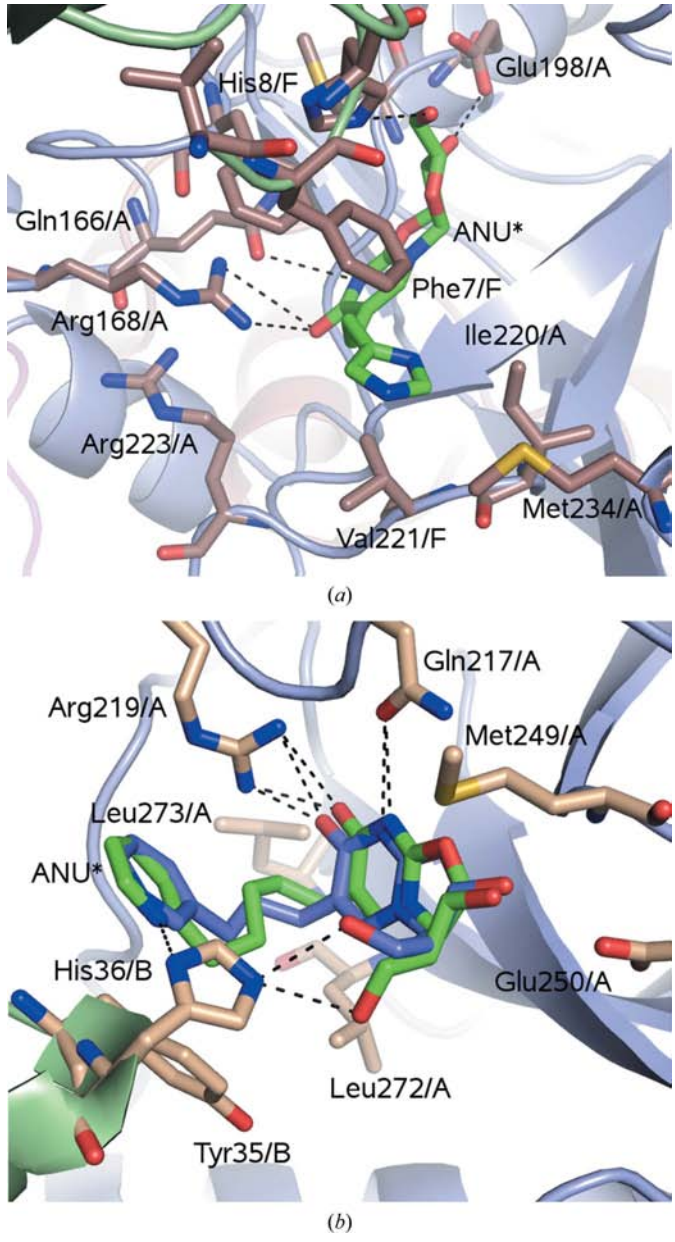

Figure 7
In silico design of ANU-based inhibitors. The major residues in the active site are shown as sticks and labelled. The virtual inhibitor in the active site of *St*UPh (*a*) and the inhibitors (containing saturated carbohydrate chains of various length) in the active centre of *H*UPhI (*b*) are shown.

No.	Structure of substituent, *St*UPh, closed conformation	G-score of the best conformer	Structure of substituent, *St*UPh, open conformation	G-score of the best conformer	Structure of substituent, *H*UPhI	G-score of the best conformer
1		−6.36	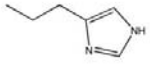	−9.02	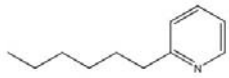	−10.84
2		−6.20	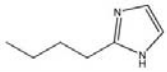	−8.92	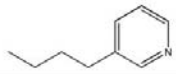	−10.49
3		−5.85	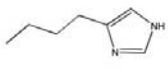	−8.83	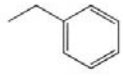	−10.42
4		−5.67	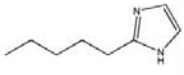	−8.81	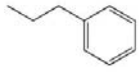	−10.42
5		−5.63	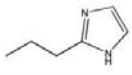	−8.68	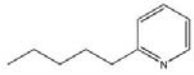	−10.34
6	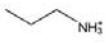	−5.48	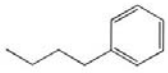	−8.67	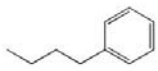	−10.11
ANU crystal		**−6.04**				
ANU dock				**−5.58**		**−5.03**

Figure 8
The best substituents at position 5 of ANU.

et al., 2009). The position of the 'core' of a putative inhibitor was set using 'Restrain' limitations (r.m.s.d. tolerance = 1 Å) in *CombiGlide*. For the binding sites in the open active centre and for the human enzyme we employed the ANU structures generated by docking procedures (see §3.5.1). The resulting docking solutions were filtered using the 'DrugLike' filter of *CombiGlide*. Three series of putative inhibitors were analyzed, each for one structure of the target enzyme. 14 structures were selected for the closed active centre of *St*UPh, 313 structures were selected for *St*UPh with an open active centre and 311 tentative structures were retrieved for *H*UPhI. The solutions were clustered, the structures presented in individual rosters were excluded and virtual compounds were docked into all three structures of the enzyme. The limitations on the positions of the 'core' moiety were the same as in the molecular design (see above). For the closed active centre of *St*UPh the procedure points to only short linear substituents because the positions of Phe7 and residues 227–230 of the L2 loop are similar to those in the X-ray structure of the *St*UPh–ANU complex.

The results of molecular design of inhibitors for the open conformation of the *St*UPh active centre (Figs. 7 and 8) and HUPhI (Fig. 8) are in agreement with the X-ray data on the binding of drugs to the phenyl substituent at position 5 of the uracil ring (BAU and structurally similar compounds; Bu *et al.*, 2005). The differences in the constructed substituents (Fig. 8) can be attributed to the variability in the conformations and primary structure of the loop (residues 223–233 in *St*UPh and 275–284 in *H*UPhI) as well as to different positioning of the side group (Phe7 in *St*UPh *versus* Tyr35 in *H*UPhI). The hydrophobic interactions of benzyl and pyridine substituents with the pocket of the *H*UPhI uracil binding site are likely to explain the inhibitor–target binding. The imidazole group of the designed *St*UPh inhibitor forms stacking interactions with Phe7 in *St*UPh, whereas this interaction is less pronounced for the pyridine group of the proposed *H*UPhI inhibitor and Tyr35 in *H*UPhI. In turn, the N atom of the pyridine group of the virtual *H*UPhI inhibitor carrying substituent 1 (Fig. 8) forms a hydrogen bond to His36*B* ND1 of *H*UPhI.

Although *H*UPhI is an attractive target for anticancer therapy, caution is required in the clinical application of these inhibitors. Recent studies have provided important evidence of the role of *H*UPhI in the central nervous system. Indeed, high uridine content in neurons protected these cells from hypoxic lesions during ischaemic stroke (Choi *et al.*, 2008). Down-regulation of *H*UPhI can decrease the amount of uridine in neurons, thereby potentiating post-stroke brain dystrophy (Balestri *et al.*, 2007). These findings indicate that *H*UPhI antagonists may not be free from side effects, in particular in elderly patients. Thus, *in silico* drug design based on bacterial models must be evaluated taking into account the manifold manifestations of *H*UPhI inhibition.

References

Adams, P. D., Grosse-Kunstleve, R. W., Hung, L.-W., Ioerger, T. R., McCoy, A. J., Moriarty, N. W., Read, R. J., Sacchettini, J. C., Sauter, N. K. & Terwilliger, T. C. (2002). *Acta Cryst.* D**58**, 1948–1954.

Balestri, F., Barsotti, C., Lutzemberger, L., Camici, M. & Ipata, P. L. (2007). *Neurochem. Int.* **51**, 517–523.

Beck, D. A. & O'Donovan, G. A. (2008). *Curr. Microbiol.* **56**, 162–167.

Berman, H. M., Henrick, K. & Nakamura, H. (2003). *Nature Struct. Biol.* **10**, 980.

Bernstein, F. C., Koetzle, T. F., Wiliams, G. J. B., Meyer, E. F. Jr, Brice, M. D., Rogers, J. R., Kennard, O., Shimanouchi, T. & Tasumi, M. (1977). *J. Mol. Biol.* **112**, 535–542.
Bu, W., Settembre, E. C., el Kouni, M. H. & Ealick, S. E. (2005). *Acta Cryst.* D**61**, 863–872.
Burling, F. T., Kniewel, R., Buglino, J. A., Chadha, T., Beckwith, A. & Lima, C. D. (2003). *Acta Cryst.* D**59**, 73–76.
Caradoc-Davies, T. T., Cutfield, S. M., Lamont, I. L. & Cutfield, J. F. (2004). *J. Mol. Biol.* **337**, 337–354.
Chandana, S. R. & Conley, B. A. (2009). *Curr. Opin. Oncol.* **21**, 218–223.
Choi, J. W., Shin, C. Y., Choi, M. S., Yoon, S. Y., Ryu, J. H., Lee, J. C., Kim, W. K., el Kouni, M. H. & Ko, K. H. (2008). *J. Neurotrauma*, **25**, 695–707.
Dontsova, M. V., Savochkina, Y. A., Gabdoulkhakov, A. G., Baidakov, S. N., Lyashenko, A. V., Zolotukhina, M., Errais Lopes, L., Garber, M. B., Morgunova, E. Y., Nikonov, S. V., Mironov, A. S., Ealick, S. E. & Mikhailov, A. M. (2004). *Acta Cryst.* D**60**, 709–711.
el Kouni, M. H., Naguib, F. N., Chu, S. H., Cha, S. M., Ueda, T., Gosselin, G., Imbach, J. L., Shealy, Y. F. & Otter, B. A. (1988). *Mol. Pharmacol.* **34**, 104–110.
el Kouni, M. H., Naguib, F. N., Niedzwicki, J. G., Iltzsch, M. H. & Cha, S. (1988). *J. Biol. Chem.* **263**, 6081–6086.
Emsley, P. & Cowtan, K. (2004). *Acta Cryst.* D**60**, 2126–2132.
Friesner, R. A., Murphy, R. B., Repasky, M. P., Frye, L. L., Greenwood, J. R., Halgren, T. A., Sanschagrin, P. C. & Mainz, D. T. (2006). *J. Med. Chem.* **49**, 6177–6196.
Gieringer, J. H., Wenz, A. F., Just, H. M. & Daschner, F. D. (1986). *Chemotherapy*, **32**, 418–424.
Iigo, M., Nishikata, K., Nakajima, Y., Szinai, I., Veres, Z., Szabolcs, A. & De Clercq, E. (1990). *Biochem. Pharmacol.* **39**, 1247–1253.
Jimenez, B. M., Kranz, P., Lee, C. S., Gero, A. M. & O'Sullivan, W. J. (1989). *Biochem. Pharmacol.* **38**, 3785–3789.
Kabsch, W. (2001). *International Tables for Crystallography*, Vol. *F*, edited by M. G. Rossmann & E. Arnold, pp. 218-225. Dordrecht: Kluwer Academic Publishers.
Kemeny, N. (1987). *Semin. Surg. Oncol.* **3**, 190–214.
Kohne, C. H. & Lenz, H. J. (2009). *Oncologist*, **14**, 478–488.
Larkin, M. A., Blackshields, G., Brown, N. P., Chenna, R., McGettigan, P. A., McWilliam, H., Valentin, F., Wallace, I. M., Wilm, A., Lopez, R., Thompson, J. D., Gibson, T. J. & Higgins, D. G. (2007). *Bioinformatics*, **23**, 2947–2948.
Lashkov, A. A., Zhukhlistova, N. E., Gabdulkhakov, A. G. & Mikhailov, A. M. (2009). *Crystallogr. Rep.* **54**, 267–278.
Laskowski, R. A., MacArthur, M. W., Moss, D. S. & Thornton, J. M. (1993). *J. Appl. Cryst.* **26**, 283–291.
Lee, C. S., Jimenez, B. M. & O'Sullivan, W. J. (1988). *Mol. Biochem. Parasitol.* **30**, 271–277.
Matsusaka, S., Yamasaki, H., Fukushima, M. & Wakabayashi, I. (2007). *Chemotherapy*, **53**, 36–41.
McCoy, A. J. (2007). *Acta Cryst.* D**63**, 32–41.
Mikhailov, A. M., Smirnova, E. A., Tsuprun, V. L., Tagunova, I. V., Vainshtein, B. K., Linkova, E. V., Komissarov, A. A., Siprashvili, Z. Z. & Mironov, A. S. (1992). *Biochem. Int.* **26**, 607–615.
Molchan, O. K., Dmitrieva, N. A., Romanova, D. V., Lopes, L. E., Debabov, V. G. & Mironov, A. S. (1998). *Biochemistry (Mosc.)*, **63**, 195–199.
Morgunova, E., Mikhailov, A. M., Popov, A. N., Blagova, E. V., Smirnova, E. A., Vainshtein, B. K., Mao, C., Armstrong, S. R., Ealick, S. E., Komissarov, A. A., Linkova, E. V., Burlakova, A. A., Mironov, A. S. & Debabov, V. G. (1995). *FEBS Lett.* **367**, 183–187.
Murshudov, G. N., Vagin, A. A. & Dodson, E. J. (1997). *Acta Cryst.* D**53**, 240–255.
Niedzwicki, J. G., el Kouni, M. H., Chu, S. H. & Cha, S. (1983). *Biochem. Pharmacol.* **32**, 399–415.
Paege, L. M. & Schlenk, F. (1952). *Arch. Biochem. Biophys.* **40**, 42–49.
Ramachandran, G. N., Ramakrishnan, C. & Sasisekharan, V. (1963). *J. Mol. Biol.* **7**, 95–99.
Roosild, T. P., Castronovo, S., Fabbiani, M. & Pizzorno, G. (2009). *BMC Struct. Biol.* **9**, 14.
Schüttelkopf, A. W. & van Aalten, D. M. F. (2004). *Acta Cryst.* D**60**, 1355–1363.
Temmink, O. H., de Bruin, M., Laan, A. C., Turksma, A. W., Cricca, S., Masterson, A. J., Noordhuis, P. & Peters, G. J. (2006). *Int. J. Biochem. Cell Biol.* **38**, 1759–1765.
Timofeev, V. I., Lashkov, A. A., Gabdoulkhakov, A. G., Pavlyuk, B. P., Kachalova, G. S., Betzel, C., Morgunova, E. Y., Zhukhlistova, N. E. & Mikhailov, A. M. (2007). *Acta Cryst.* F**63**, 852–854.
Xie, X. Q. & Chen, J. Z. (2008). *J. Chem. Inf. Model.* **48**, 465–475.
Yamashiro, Y., Fukuoka, Y., Yotsuji, A., Yasuda, T., Saikawa, I. & Ueda, Y. (1986). *J. Antimicrob. Chemother.* **18**, 703–708.
Zolotukhina, M., Ovcharova, I., Eremina, S., Errais Lopes, L. & Mironov, A. S. (2003). *Res. Microbiol.* **154**, 510–520.